Structure of the nematic mesophase with cybotactic groups in liquid-crystalline poly(urethane-ester)s

O. Francescangeli
Dipartimento di Scienze dei Materiali e della Terra, Università di Ancona, Via Brecce Bianche, 60131 Ancona, Italy and Istituto Nazionale per la Fisica della Materia, Unità di Ancona, Via Brecce Bianche, 60131 Ancona, Italy

M. Laus
Dipartimento di Chimica Industriale e dei Materiali, Università di Bologna, Viale Risorgimento 4, 40136 Bologna, Italy

G. Galli
Dipartimento di Chimica e Chimica Industriale, Università di Pisa, Via Risorgimento 35, 56100 Pisa, Italy
(Received 5 February 1996)

The results of a structural analysis by x-ray diffraction on fiber samples of the nematic mesophase with cybotactic groups of poly(urethane-ester) TDI-C_2C_6, TDI-C_6C_4, TDI-C_6C_6, TDI-C_6C_8, and TDI-C_6C_{10} as prepared from various mesogenic alkylene di[4-(ω-hydroxyalkyloxy-4-oxybenzoyl)oxybenzoate]s (C_mC_n; $m=2$ or 6 and $n=4$, 6, 8, or 10) and 2,4-toluenediisocyanate (TDI) are reported. Evidence is provided for the existence of two different molecular orderings within the nematic phases with cybotactic groups, to which different internal degrees of correlation correspond. The average dimension of the cybotactic clusters along the director is comprised between ~260 and ~560 Å, whereas the average dimension perpendicular to the director ranges from ~130 to ~270 Å. Accordingly, the cybotactic clusters present an asymmetrical ellipsoidal-like shape. On the other hand, the correlation length within the nematic liquid crystal surrounding the cybotactic clusters and along the director is between 38 and 45 Å. These values are of the order of the molecular length. These findings highlight the multidomain nature of the mesophase consisting of large and asymmetric clusters surrounded by a conventional nematic endowed with a very low correlation degree. [S1063-651X(97)02801-8]

PACS number(s): 61.30.Eb, 61.10.Eq, 61.10.Ht

I. INTRODUCTION

In recent papers [1,2] we have reported on the synthesis and mesomorphic behavior of poly(urethane-ester) TDI-C_mC_n of the following structure:

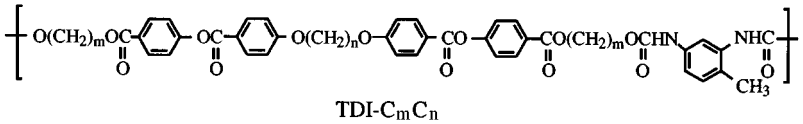

TDI-C_mC_n
(m = 2, 4, or 6;
n = 4, 6, 8, or 10)

(where TDI denotes 2,4-toluenediisocyanate). All poly(urethane-ester)s TDI-C_mC_n were amorphous. Samples TDI-C_2C_6, TDI-C_6C_4, and TDI-C_6C_{10} displayed one mesophase, whereas two mesophases were detected for samples TDI-C_4C_6, TDI-C_6C_6, and TDI-C_6C_8. The diffraction patterns obtained on stretched oriented fibers of TDI-C_2C_6, TDI-C_6C_4, and TDI-C_6C_{10}, drawn at a temperature within the mesophasic range, and for TDI-C_4C_6, TDI-C_6C_6, and TDI-C_6C_8, at temperatures inside the lower temperature mesophase, showed the formation of a nematic mesophase with cybotactic groups. In contrast, diffraction spectra typical of a conventional nematic mesophase were recorded for fibers drawn at temperatures inside the higher-temperature mesophase of the latter set of poly(urethane-ester)s. These findings indicated the formation of one nematic mesophase with cybotactic groups in polymers TDI-C_2C_6, TDI-C_6C_4, and TDI-C_6C_{10} and two sequential nematic mesophases in polymers TDI-C_4C_6, TDI-C_6C_6, and TDI-C_6C_8, namely, nematic with cybotactic groups at low temperature and conventional nematic at high temperature, connected by a first-order transition. Accordingly, these poly(urethane-ester)s offer an example of a class of evenly spaced main chain polymers exhibiting different nematic phases in a sequence. In addition, the analysis of the diffraction patterns of the nematic mesophase with cybotactic groups indicated that two structural arrangements, a smectic-*C*-like and a conventional nematic structure, coexist. In the following, the nematic mesophase with cybotactic groups will be referred to as ''cybotactic nematic'' mesophase for short.

To provide a detailed description of the macromolecular organization in the cybotactic nematic mesophase, in the present paper we report an x-ray-diffraction study of

poly(urethane-ester)s TDI-C_2C_6, TDI-C_6C_4, TDI-C_6C_6, TDI-C_6C_8, and TDI-C_6C_{10} samples oriented by stretching fibers at a temperature within the cybotactic mesophase range. The correlation lengths and average dimensions of the cybotactic clusters as well as the correlation lengths in the nematic surrounding them are evaluated.

II. EXPERIMENT

A. Materials

Poly(urethane-ester)s TDI-C_mC_n were obtained by a stepwise polyaddition reaction of mesogenic diols C_mC_n, consisting of two *p*-oxybenzoyl diads interconnected by a polymethylene segment containing n ($n=4$, 6, 8, or 10) methylene groups and flanked by two linear ω-hydroxyalkylene segments containing m ($m=2$, 4, or 6) methylene groups, with commercial 2,4-toluenediisocyanate in chloroform solution at 90 °C for 48 h, as described in detail elsewhere [2].

B. Characterization

X-ray-diffraction photographs on oriented samples were obtained by means of a conventional x-ray powder diffractometer equipped with a pinhole flat-plate camera with a temperature controlled cell (±0.1 °C). Ni-filtered Cu $K\alpha$ radiation ($\lambda=1.54$ Å) was used. Fibers were oriented by pulling up with tweezers the viscous liquid-crystalline melt at different temperatures throughout the entire mesophase range, or the isotropic melt at 440 K, and cooling them in air at room temperature. For all the samples x-ray-diffraction patterns of the oriented mesophases were taken at room temperature and at temperatures in the 360–370 K range. Intensity contour maps and intensity profiles along specified directions in the reciprocal space were obtained by digitalizing the x-ray-diffraction patterns, using the Kodak photo–compact disc system, and elaborating the digitalized numerical signal by NIH Image (version 1.55, public domain) and Spyglass Transform image processing programs. The numerical calculations from the x-ray spectra were performed after background subtraction, correction for the usual technical factors such as the Lorentz factor, and deconvolution for the instrumental resolution function.

III. RESULTS AND DISCUSSION

The thermal behavior of poly(urethane-ester)s TDI-C_2C_6, TDI-C_6C_4, TDI-C_6C_6, TDI-C_6C_8, and TDI-C_6C_{10} has been reported previously [1,2]. At room temperature, all the samples are amorphous and the liquid-crystalline behavior extends from the glass transition to the nematic-isotropic transition. TDI-C_2C_6, TDI-C_6C_4, and TDI-C_6C_{10} show the glass transition at 362, 337, and 328 K, respectively, and an endothermic peak centered at 424 K ($\Delta S_i=8.7$ J mol^{-1} K^{-1}), 431 K ($\Delta S_i=25.5$ J mol^{-1} K^{-1}), and 394 K ($\Delta S_i=36.0$ J mol^{-1} K^{-1}), respectively, attributed to the isotropization. TDI-C_6C_6 and TDI-C_6C_8 show the glass transition at 333 and 322 K, respectively. In addition, both samples exhibit two endothermic peaks at 412 K ($\Delta S_{N\text{-}N'}=10.7$ J mol^{-1} K^{-1}) and 415 K ($\Delta S_i=15.9$ J mol^{-1} K^{-1}) for TDI-C_6C_6 and at 390 K ($\Delta S_{N\text{-}N'}=6.4$ J mol^{-1} K^{-1}) and 395 K ($\Delta S_i=15.7$ J mol^{-1} K^{-1}) for TDI-C_6C_8. The lower-temperature transition is attributed to a transition between two nematic mesophases and the higher-temperature transition to the isotropization.

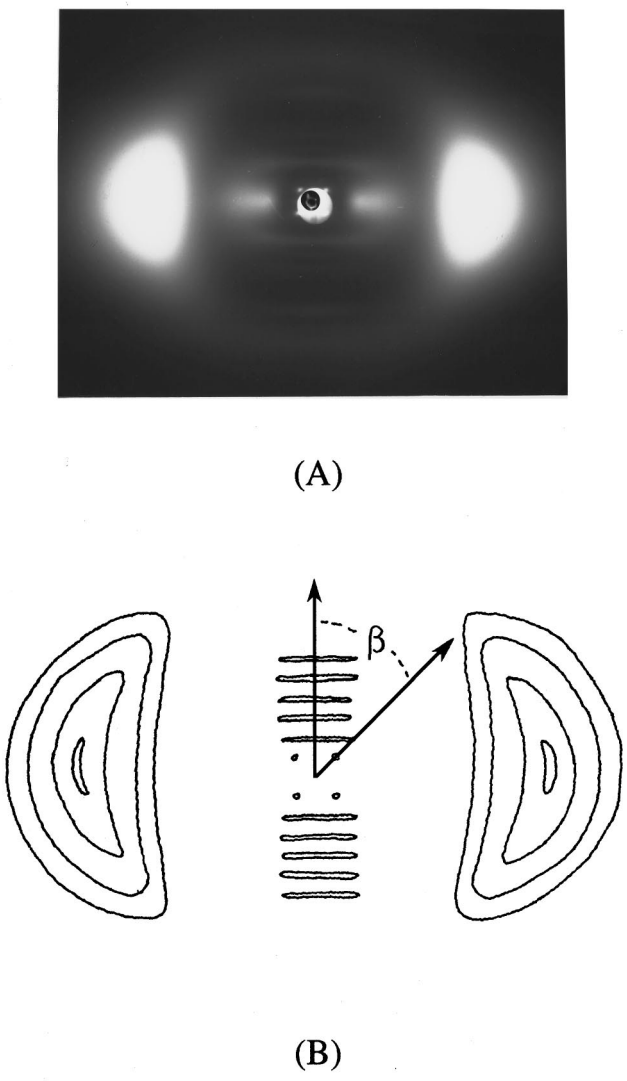

FIG. 1. (a) X-ray-diffraction pattern of the oriented mesophase of polymer TDI-C_6C_4 at $T=360$ K and (b) schematic representation of its intensity contour map. (Vertical fiber axis; sample to film distance 75 mm.) A very similar pattern was recorded at room temperature.

For each sample the fiber diffraction pattern taken at a temperature within the range 360–370 K was found to be very similar to the room-temperature fiber diffraction pattern, thus indicating that in the fiber samples at room temperature the cybotactic nematic molecular organization is frozen in below the glass transition. In addition, the x-ray-diffraction spectra of the oriented mesophases of samples TDI-C_2C_6, TDI-C_6C_4, and TDI-C_6C_{10} and the diffraction spectra of fibers of TDI-C_6C_6 and TDI-C_6C_8 oriented at a temperature corresponding to the existence range of the lower-temperature nematic mesophase are very similar. As a typical example, the x-ray-diffraction pattern of sample TDI-C_6C_4 at $T=360$ K is shown in Fig. 1 together with the schematic representation of the contour map. The diffraction pattern consists of two symmetrically placed wide-angle broad crescents centered on the equator, associated with the

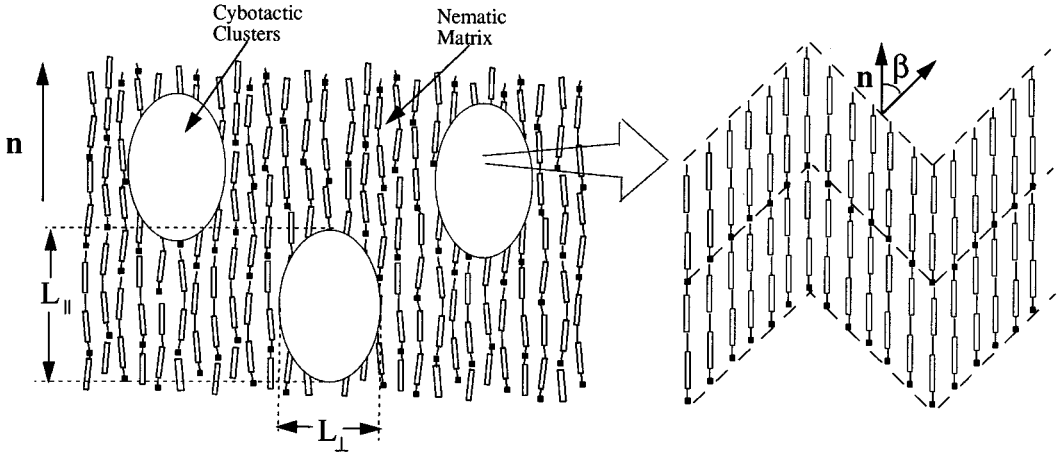

FIG. 2. Schematic representation of the structural arrangements of the polymer chains in the cybotactic nematic mesophase.

liquidlike short-range ordering, corresponding to an interchain average distance of $D \approx 4.7$ Å, and four sharp small-angle spots symmetrically placed about the direct beam and forming pairs on a straight line at an angle β with respect to the meridional line (i.e., the fiber axis). In addition, a small fraction of the scattered intensity is localized on regularly spaced diffuse lines situated in the direction perpendicular to the fiber axis. No correlation exists between the spacing of these diffuse lines and the position of the strong off-meridional maxima.

The above x-ray-diffraction spectra were previously attributed [1] to the presence of a nematic mesophase with local smectic-*C*-like fluctuations. According to this model, the small-angle four-spot pattern is the result of the x-ray scattering from tilted planar groupings of parallel vertical macromolecules in a smectic-*C*-like arrangement [3,4]. The regularly spaced diffuse lines perpendicular to the meridional direction and symmetrically placed above and below the equatorial line were attributed [1] to the coherent diffuse intermolecular scattering associated with the uncorrelated longitudinal positional disorder of the chains. These experimental findings indicate that two structural arrangements, namely, a smectic-*C*-like and a conventional nematic structure, coexist within the cybotactic mesophase of these poly(urethane-ester)s. A schematic model of the structural arrangements of the polymer chains in the cybotactic mesophase is reported in Fig. 2. However, as pointed out in a previous paper [1], the analysis of the x-ray-diffraction data did not allow us to distinguish whether this is a static situation or rather a dynamic equilibrium where small nematic regions fluctuate to and from the smecticlike arrangement (order parameter fluctuations).

Further information concerning the molecular organization in the nematic cybotactic mesophase can be obtained from the analysis of the low-angle region of the spectra of the oriented samples. The layer spacing d and the tilt angle β of the layered structures in the cybotactic clusters are obtained from the position of the four-spot pattern. From the values of the spacing d and the tilt angle β, it is possible to calculate the length of the repeating unit L_{expt} in the cybotactic nematic, which can be compared to the corresponding values L_{calc} calculated from standard atomic bond lengths and angles considering the molecule in the planar fully extended conformation (Table I). Good agreement between L_{expt} and L_{calc} is observed. L_{expt} increases with increasing length of both the flexible spacers and a value of 2.7 Å for the projection of two C–C bonds in the polymethylene chain can be estimated, which is very close to the value 2.54 Å of the projection of two carbon bonds in a polymethylene chain [5]. Therefore, the conformation of the polymethylene spacers does not depart considerably from the fully extended one, independently of their position in the polymer repeat unit.

The correlation lengths and the average dimensions of the cybotactic clusters can be obtained from the analysis of the intensity profile of the small-angle four-spot pattern in the directions parallel and normal to the director axis **n**, respectively. Figure 3 shows the contours of constant intensity of the small-angle region of the diffraction spectrum of TDI-C_6C_{10}. We denote by $q_\parallel$ and $q_\perp$ the longitudinal (parallel to the director **n**) and transversal (orthogonal to **n**) components, respectively, of the scattering vector **q** in the reciprocal space (whose modulus is $q = 4\pi \sin\theta/\lambda$, 2θ being the scattering angle) and by $\mathbf{q}_0$ the scattering vector corresponding to the maximum intensity ($q_0 = 4\pi \sin\theta_B/\lambda$, θ_B being the Bragg angle). The scattered intensity I as a function of $q_\parallel$ was measured by performing an optical density scan of the x-ray-diffraction spectrum along the direction parallel to the fiber axis keeping $q_\perp$ constant at $q_\perp = q_{0\perp}$. This condition was met by performing a scan with the scattering vector **q** moving along the straight line through $\mathbf{q}_0$ and parallel to **n** (Fig. 3). This direction is identified in the reciprocal space by either one of the two vertical straight lines aa' and bb'. The corresponding intensity profile $I(q_\parallel, q_{0\perp})$ was obtained by measuring the optical density of the x-ray-diffraction spectra along these two straight lines. Similarly, the scattered inten-

TABLE I. X-ray-diffraction data of polyurethanes TDI-C_mC_n.

Sample	β (deg)	d (Å)	L_{expt} (Å)	L_{calc} (Å)
TDI-C_2C_6	46.4	32.2	46.7	48.5
TDI-C_6C_4	49	36.4	55.5	55
TDI-C_6C_6	46.4	39.4	57.1	58.5
TDI-C_6C_8	50	38.5	59.9	61
TDI-C_6C_{10}	54.2	37.3	63.8	63.5

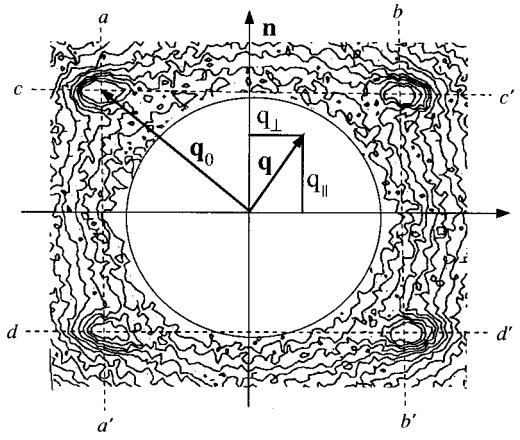

FIG. 3. Contours of constant intensity in the small-angle region of the diffraction spectrum of TDI-C_6C_{10}.

sity as a function of $q_\perp$ was obtained by performing a scan with the scattering vector **q** moving on the straight line passing through $\mathbf{q}_0$ and normal to the director **n**. This direction is identified in the reciprocal space by either one of the two straight lines cc' an dd' shown in Fig. 3. As an example, Figs. 4(a) and 4(b) show $I(q_\parallel, q_{0\perp})$, measured along the section aa', and $I(q_{0\parallel}, q_\perp)$, measured along the section cc′, respectively, of sample TDI-C_6C_{10}. Similar curves were obtained by performing the measurement along the sections bb' and dd', respectively. The filled circles in Figs. 5(a) and 5(b) show the experimental intensity profiles $I(q_\parallel)=I(q_\parallel, q_{0\perp})$ and $I(q_\perp)=I(q_{0\parallel}, q_\perp)$, respectively, about the vector $\mathbf{q}_0$ for the right spot on the upper side of Fig. 3 of sample TDI-C_6C_{10}. These data were obtained from Fig. 4, after background subtraction and normalization of the peak

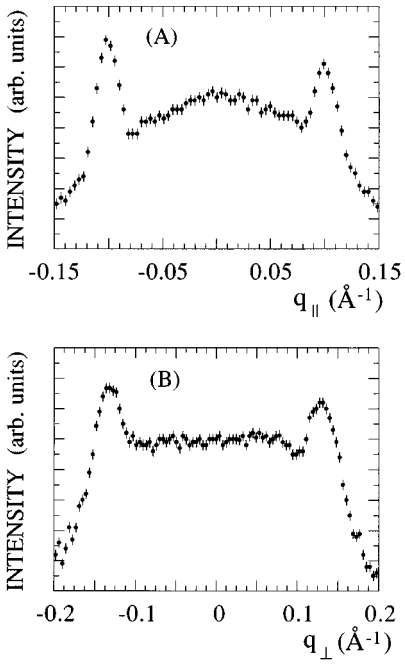

FIG. 4. (a) Intensity profile $I(q_\parallel)=I(q_\parallel, q_\perp=q_{0\perp})$ and (b) intensity profile $I(q_\perp)=I(q_\parallel=q_{0\parallel}, q_\perp)$ of sample TDI-C_6C_{10} measured along the sections aa' and cc', respectively.

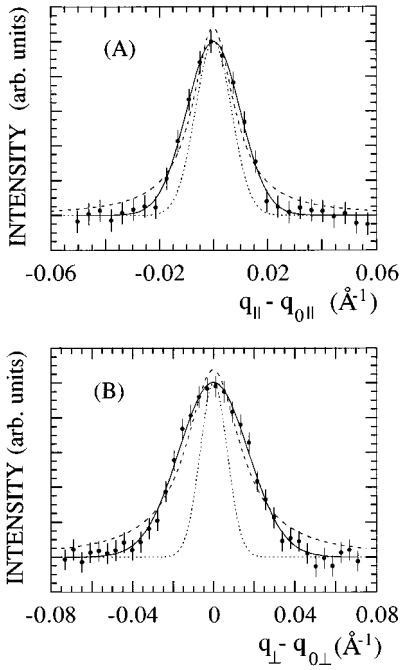

FIG. 5. (a) Intensity profile $I(q_\parallel - q_{0\parallel})$ and (b) intensity profile $I(q_\perp - q_{0\perp})$ of sample TDI-C_6C_{10} obtained from the spectra of Fig. 4 after background subtraction: $q_{0\parallel}=0.0985$ Å^{-1} and $q_{0\perp}=0.1366$ Å^{-1}. The full circles are the experimental data and the continuous lines give the best fit by a Gaussian function. The dashed lines represent the best fit by a Lorentzian function. The Gaussian dotted curves represent the resolution function of the experimental apparatus.

intensity to one. Very similar profiles were obtained for the other spots.

The best fits of these intensity profiles for all the samples were obtained by using a Gaussian function. As an example, the continuous lines in Figs. 5(a) and 5(b) give the Gaussian best fits to the experimental data. In any case, the intensity distribution about $\mathbf{q}_0$ was then written in the form of the two-dimensional Gaussian function, described by

$$I(q_\parallel, q_\perp)=I_0\exp\left\{-\left[\frac{(q_\parallel-q_{0\parallel})^2}{2\Delta q_\parallel^2}+\frac{(q_\perp-q_{0\perp})^2}{2\Delta q_\perp^2}\right]\right\}. \quad (1)$$

Accordingly, the longitudinal and transversal intensity distributions $I(q_\parallel)=I(q_\parallel, q_\perp=q_{0\perp})$ and $I(q_\perp)=I(q_\parallel=q_{0\parallel}, q_\perp)$ were then fitted as described by

$$I(q_\parallel)=I_0\exp\left[-\frac{(q_\parallel-q_{0\parallel})^2}{2\Delta q_\parallel^2}\right] \quad (2)$$

and

$$I(q_\perp)=I_0\exp\left[-\frac{(q_\perp-q_{0\perp})^2}{2\Delta q_\perp^2}\right]. \quad (3)$$

The values of the parameters $\Delta q_\parallel$ and $\Delta q_\perp$ obtained by fitting Eqs. (2) and (3) to the experimental data are reported in Table II. The correlation lengths in the real space can be estimated once the correlation function in the real space is determined. The latter was obtained by Fourier inversion of the diffracted intensity distribution after correction for the

TABLE II. Parameters obtained by fitting the intensity profiles $I(q_\parallel - q_{0\parallel}) = I(q_\parallel - q_{0\parallel}, q_\perp = q_{0\perp})$ and $I(q_\perp - q_{0\perp}) = I(q_\parallel = q_{0\parallel}, q_\perp - q_{0\perp})$ of all the samples by using Eqs. (2) and (3), respectively. $\Delta q_{\parallel d}$ and $\Delta q_{\perp d}$ are the values of $\Delta q_\parallel$ and $\Delta q_\perp$ after deconvolution for the instrumental resolution function. $\zeta_\parallel$ and $\zeta_\perp$ are the longitudinal and transversal correlation length, respectively, in the cybotactic clusters. The numbers in parentheses are the errors on the last significant digit.

Sample	$\Delta q_\parallel$ (Å^{-1})	$\Delta q_\perp$ (Å^{-1})	$\Delta q_{\parallel d}$ (Å^{-1})	$\Delta q_{\perp d}$ (Å^{-1})	$\xi_\parallel$ (Å)	$\xi_\perp$ (Å)
TDI-C_2C_6	0.0175(4)	0.0340(8)	0.0160(5)	0.0333(9)	88(3)	43(1)
TDI-C_6C_4	0.0165(4)	0.0176(4)	0.0149(5)	0.0161(5)	95(3)	88(3)
TDI-C_6C_6	0.0146(4)	0.0172(4)	0.0128(5)	0.0157(5)	110(4)	90(3)
TDI-C_6C_8	0.0125(4)	0.0172(4)	0.0104(5)	0.0157(5)	136(7)	90(3)
TDI-C_6C_{10}	0.0104(3)	0.0172(4)	0.0076(4)	0.0156(5)	186(11)	91(3)

resolution of the experimental apparatus. The dotted lines in Fig. 5 show the instrumental resolution function, which is represented by a Gaussian curve of full width at half maximum (FWHM) $\Delta q^{\mathrm{FWHM}} = 0.0166(2)$ Å^{-1} in both the longitudinal and transversal directions.

Then, the intensity distributions $I(q_\parallel)$ and $I(q_\perp)$ after deconvolution for the instrumental resolution function are still Gaussian functions described by

$$I(q_{\parallel,\perp}) = I_0 \exp\left[-\frac{(q_{\parallel,\perp} - q_{0\parallel,0\perp})^2}{2\Delta q^2_{\parallel d,\perp d}} \right], \tag{4}$$

where

$$\Delta q_{\parallel d,\perp d} = \sqrt{(\Delta q^2_{\parallel,\perp} - \Delta q^2_{\mathrm{res}})} \tag{5}$$

and the parameter Δq_{res} of the resolution function is simply $\Delta q_{\mathrm{res}} = \Delta q^{\mathrm{FWHM}}/2\sqrt{2}\sqrt{\ln 2} = 7.079 \times 10^{-3}$ Å^{-1}. The values of $\Delta q_{\parallel d}$ and $\Delta q_{\perp d}$ are reported in Table II.

The Gaussian profile of the small-angle reflections has an important consequence in connection with the physical problem concerning the static or dynamic nature of the smectic order in the cybotactic clusters. In fact, if the small-angle four-spot pattern were due to the order parameter fluctuations of nematic regions from and to the smecticlike arrangement we should expect an intensity profile, after deconvolution of the experimental data for the instrumental resolution function, described by an equation having the form

$$I(q_\parallel, q_\perp) = \frac{I_0}{1 + \xi^2_\parallel (q_\parallel - q_{0\parallel})^2 + \xi^2_\perp (q_\perp - q_{0\perp})^2 [1 + c\xi^2_\perp (q_\perp - q_{0\perp})^2]}, \tag{6}$$

where $\xi_\parallel$ and $\xi_\perp$ define the longitudinal and transversal correlation lengths, respectively, and c is a constant. Equation (6) with $c = 0$ gives the two-dimensional Lorentzian shape of the scattered intensity from the order-parameter fluctuations as predicted by the Landau theory [6] of the nematic-smectic phase transition proposed by McMillan [7] and de Gennes [8]. A value of the parameter c different from zero allows us to include a fourth-order correction in $(q_\perp\text{-}q_0)$ to the scattering cross section, as found by Als-Nielsen *et al.* [9] and consistent with the Chen-Lubensky theory [10,11]. This theory, based on the nematic–smectic-*A* or -*C* Lipshitz model, predicts that the scattered intensity due to the order parameter fluctuations in the nematic–smectic-*C* pretransitional region is described in the measuring plane by a Lorentzian function in the longitudinal direction and a modified Lorentzian function in the transverse direction according to Eq. (6) (under the assumption that the variation of the molecular structure factor over the region of reciprocal space investigated could be neglected).

It should be noted that for all the samples investigated it was impossible to obtain a satisfactory fit of the experimental data using the Lorentzian-type curve of Eq. (6) [for comparative purposes see the dashed lines in Figs. 5(a) and 5(b)]. On the other hand, a Gaussian line shape of the diffraction peaks is often found when the short-range order of the smectic domains originates from the positional disorder of the molecular units [12]. Thus order parameter fluctuations appear not to be the origin of the small-angle four-spot signal for the smectic-*C*-like arrangement, which seems to arise from a static situation rather than a dynamic equilibrium involving correlation fluctuations driven by the long segmented mesogenic units [1].

The Fourier inversion of Eq. (4) gives the shape of the correlation functions parallel and normal to the director in the real space as described by

$$G_\parallel(z) = \exp\left(-\frac{z^2 \Delta q^2_{\parallel d}}{2} \right) = \exp\left(-\frac{z^2}{\xi^2_\parallel} \right) \tag{7}$$

and

$$G_\perp(r) = \exp\left(-\frac{r^2 \Delta q^2_{\perp d}}{2} \right) = \exp\left(-\frac{r^2}{\xi^2_\perp} \right), \tag{8}$$

where z and r are the distances parallel and perpendicular to the director, respectively, and $\xi_\parallel$ and $\xi_\perp$ are the longitudinal and the transversal correlation lengths, respectively. The values of $\xi_\parallel$ and $\xi_\perp$ obtained for all samples are reported in Table II. Figure 6 shows the trend of the correlation lengths

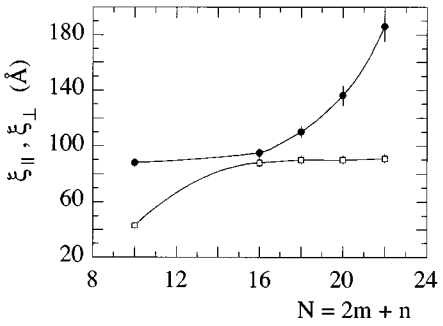

FIG. 6. Trend of the correlation lengths $\xi_{\parallel}$ (full dots) and $\xi_{\perp}$ (open squares) as a function of the number N of methylene groups in the repeating unit $N=2m+n$.

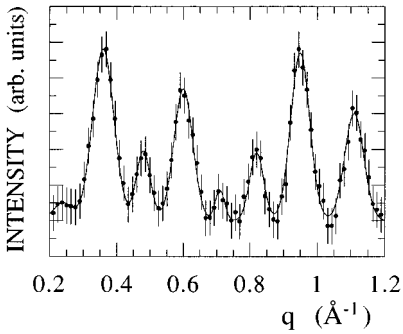

FIG. 7. Intensity of the diffuse reflections along the meridional line of sample TDI-C_6C_6. The continuous line gives the best fit to the experimental data by a superposition of Lorentzian functions.

$\xi_{\parallel}$ and $\xi_{\perp}$ as a function of the overall number N of methylene groups in the repeating unit ($N=2m+n$). A regular increase in the longitudinal correlation length $\xi_{\parallel}$ with increasing N is observed, whereas the transversal correlation length $\xi_{\perp}$ initially increases as N increases and then reaches a constant value of about 90 Å. The increase in the longitudinal correlation length $\xi_{\parallel}$ with increasing length of the flexible spacer clearly indicates an effective participation of the flexible spacer in the ordering process in the nematic mesophase.

A reliable estimate of the average longitudinal $L_{\parallel}$ and transversal $L_{\perp}$ (Fig. 2) dimensions of the cybotactic clusters can be obtained by considering the longitudinal and transversal distances (in the real space) which correspond to the correlation extinction. For a Gaussian function, the correlation conventionally vanishes after three times the correlation length. Then, from the definition of the correlation lengths [see Eqs. (7) and (8)] it follows that

$$L_{\parallel,\perp}=3\,\frac{\sqrt{2}}{\Delta q_{\parallel d,\perp d}}=\frac{6\sqrt{\ln 2}}{\pi}\,\frac{\lambda}{\Delta(2\theta)_{\parallel,\perp}\cos\theta_B}$$
$$=1.59\,\frac{\lambda}{\Delta(2\theta)_{\parallel,\perp}\cos\theta_B}, \qquad (9)$$

where λ is the wavelength of the incident radiation, θ_B is the Bragg angle, and $\Delta(2\theta)_{\parallel}$ and $\Delta(20)_{\perp}$ are the FWHMs of the diffraction peak measured in the longitudinal and transversal direction. This equation is formally equal to the Scherrer equation [13]:

$$L_{\parallel,\perp}=K\,\frac{\lambda}{\Delta(2\theta)_{\parallel,\perp}\,\cos\theta_B}, \qquad (10)$$

TABLE III. Longitudinal $L_{\parallel}$ and transversal $L_{\perp}$ dimensions of the cybotactic clusters estimated as three times the corresponding correlation length.

Sample	$L_{\parallel}$ (Å)	$L_{\perp}$ (Å)
TDI-C_2C_6	264(9)	129(3)
TDI-C_6C_4	285(10)	264(9)
TDI-C_6C_6	330(12)	270(9)
TDI-C_6C_8	408(20)	270(9)
TDI-C_6C_{10}	558(32)	273(9)

where the coefficient K is 1.59. This value is intermediate between the values 0.9 and 1.84, as expected for a perfect crystal and a disordered layer lattice [14], respectively. The average dimensions of the cybotactic clusters calculated by means of Eq. (9) are summarized in Table III.

Further information about the ordering in the nematic region can be obtained from the analysis of the diffuse scattering in the small-angle region. The diffuse streaks, orthogonal to the director and located along the meridional line, correspond to the intersection with the Ewald sphere of a series of equidistant diffuse planes representing the Fourier transform of a linear modulated object oriented along the director [15]. As an example, Fig. 7 reports the experimentally measured intensity profiles of TDI-C_6C_6 along the meridional line, after background subtraction and correction for the Lorentz factor. The same type of diffuse streaks were found in the diffraction patterns of both polymeric smectic phases [16,17] and polymeric [18] and conventional nematic [19] phases and indicate that the molecules tend to align themselves in rows over a short range. The diffraction pattern for a series of parallel periodic chains with periodicity a but with a disordered net of chain centers is a series of sheets of scattering normal to the chains and spaced $1/a$ apart [20] (Fig. 8). The planar spreading of the intensity in the reciprocal space results from the longitudinal disordered arrangement of the chains. The correlation length of this ordered structure may be estimated from the width of the diffuse streaks along the director. From the measurement of the spacing between adjacent diffuse lines in the reciprocal space, it is possible to estimate the period L_{diff} of the corresponding linear lattice in the real space, which is of the order of the molecular length. The L_{diff} values obtained are significantly lower than the corresponding L_{calc} values estimated for the most extended molecular conformation. The difference $L_{\mathrm{calc}}-L_{\mathrm{diff}}$ is 4.5, 4.0, 6.5, 6.6, and 5.5 Å for TDI-C_2C_6, TDI-C_6C_4, TDI-C_6C_6, TDI-C_6C_8, and TDI-C_6C_{10}, respectively. Since the diffuse peaks arise from correlations in the molecular arrangement along the director, the most obvious explanation of this difference is in terms of a tilt effect. If we consider the mean projection of the molecular length along the director, i.e., $d=L\langle|\cos\varphi|\rangle$, we can calculate an average angle φ of the molecule from its preferred direction ($\varphi=0$) by $\varphi=\langle\cos^{-1}(d/L)\rangle$. The values of φ_{diff} so obtained are 25°, 22°, 24°, 27°, and 27° for TDI-C_2C_6, TDI-C_6C_4, TDI-C_6C_6, TDI-C_6C_8, and TDI-C_6C_{10}, respectively. These values are in

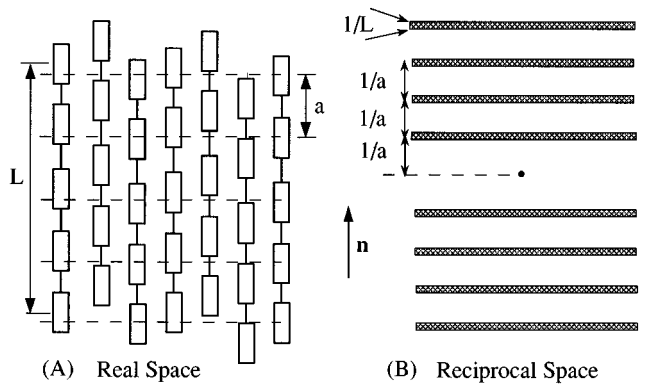

FIG. 8. Schematic representation of the structure and diffraction pattern for a system of uncorrelated rods.

good agreement with the average tilt angle usually reported in other low molar mass nematic liquid crystals [21].

From the intensity profile of the diffuse reflections along the director it is possible to estimate the longitudinal correlation length $\xi_{\parallel}$ in the nematic phase by the equation

$$\xi_{\parallel}=\frac{2}{\Delta q_{\parallel}}, \tag{11}$$

where $\Delta q_{\parallel}$ is the FWHM of the Lorentzian curves describing the shape of the diffuse reflections in the reciprocal space. The values of the longitudinal correlation lengths obtained after correction for the finite experimental resolution and averaging over the whole set of diffuse reflections are 38, 40, 42, 42, and 45 Å for samples TDI-C_2C_6, TDI-C_6C_4, TDI-C_6C_6, TDI-C_6C_8, and TDI-C_6C_{10}, respectively.

IV. CONCLUSION

The x-ray-diffraction analysis of the cybotactic nematic mesophase in several samples of main chain liquid-crystalline poly(urethane-ester)s is reported. Evidence is provided of the existence of two different molecular orderings within the cybotactic nematic phase to which different internal degrees of correlation correspond. The average dimension of the cybotactic clusters along the director is comprised between ~260 and ~ 560 Å, whereas the average dimension perpendicular to the director ranges from ~130 to ~270 Å. Accordingly, the cybotactic clusters present an asymmetrical ellipsoidal-like shape. The longitudinal correlation length increases regularly as the length of the flexible spacer increases, whereas the transversal correlation length reaches a constant value, thus clearly indicating that the flexible spacer plays a fundamental role in the ordering process in the nematic mesophase.

On the other hand, the correlation length within the nematic surrounding the cybotactic clusters and along the director is comprised between 38 and 45 Å. This value is of the order of the molecular length. These findings highlight the multidomain nature of the cybotactic nematic mesophase consisting of large and asymmetric clusters even though the correlation degree in the surrounding nematic is very low.

ACKNOWLEDGMENTS

This work was supported by the Ministero dell'Università e della Ricerca Scientifica e Tecnologica of Italy.

[1] O. Francescangeli, B. Yang, M. Laus, A. S. Angeloni, G. Galli, and E. Chiellini, J. Polym. Sci., Polym. Phys. **33**, 699 (1995).
[2] E. Chiellini, G. Galli, S. Trusendi, A. S. Angeloni, M. Laus, and O. Francescangeli, Mol. Cryst. Liq. Cryst. **243**, 135 (1994).
[3] A. DeVries, Mol. Cryst. Liq. Cryst. **10**, 219 (1970).
[4] L. V. Azaroff, Proc. Nat. Acad. Sci. U.S.A. **77**, 1252 (1980).
[5] P. J. Flory, *Statistical Mechanics of Chain Molecules* (Interscience, New York, 1969).
[6] W. L. McMillan, Phys. Rev. A **7**, 1673 (1973).
[7] W. L. McMillan, Phys. Rev. A **6**, 936 (1972).
[8] P. G. de Gennes, Solid State Commun. **10**, 753 (1972).
[9] J. Als-Nielsen, R. J. Birgeneau, M. Kaplan, J. D. Lister, and C. R. Safinya, Phys. Rev. Lett. **39**, 352 (1977).
[10] L. Chen and T. Lubensky, Phys. Rev. A **14**, 1202 (1976).
[11] C. R. Safinya, L. J. Martinez-Miranda, M. Kaplan, J. D. Lister, and R. J. Birgeneau, Phys. Rev. Lett. **50**, 56 (1983).
[12] A. J. Leadbetter, in *The Molecular Physics of Liquid Crystals*, edited by G. R. Luckhurst and G. W. Gray (Academic, London, 1979), Chap. 13.
[13] A. Guinier, *X-Ray Diffraction* (Freeman, San Francisco, 1963).
[14] B. E. Warren, Phys. Rev. **59**, 693 (1941).
[15] A. Guinier, *X-Ray Diffraction in Crystals, Imperfect Crystals and Amorphous Bodies* (Freeman, San Francisco, 1965).
[16] P. Davidson, P. Keller, and A. M. Levelut, J. Phys. (Paris) **46**, 939 (1985).
[17] P. Davidson and A. M. Levelut, J. Phys. (Paris) **50**, 2415 (1989).
[18] F. Hardouin, S. Méry, M. F. Achard, M. Mauzac, P. Davidson, and P. Keller, Liq. Cryst. **8**, 565 (1990).
[19] A. M. Levelut, Y. Fang, and C. Destrade, Liq. Cryst. **4**, 441 (1989).
[20] R. W. James, *The Optical Principles of the Diffraction of X-Rays* (Bell, London, 1948).
[21] A. De Vries, A. Ekachai, and N. Spielberg, Mol. Cryst. Liq. Cryst. **49**, 143 (1979).